Published in final edited form as:
FEBS J. 2012 March ; 279(6): 1093–1105. doi:10.1111/j.1742-4658.2012.08506.x.

Structural characterization of *H. pylori* dethiobiotin synthetase reveals differences between family members

Przemyslaw J. Porebski[1,2,7], **Maria Klimecka**[1,7], **Maksymilian Chruszcz**[1,7], **Robert A. Nicholls**[1,5,7], **Krzysztof Murzyn**[1,2,7], **Marianne E. Cuff**[4,7], **Xiaohui Xu**[3,7], **Marcin Cymborowski**[1,7], **Garib N. Murshudov**[6], **Alexei Savchenko**[3,7], **Aled Edwards**[3,7], and **Wladek Minor**[1,7,*]

[1]University of Virginia, Department of Molecular Physiology and Biological Physics, Charlottesville, VA 22908, USA [2]Department of Computational Biophysics and Bioinformatics, Jagiellonian University, 30-387 Kraków, Poland [3]Banting and Best Department of Medical Research, University of Toronto, Toronto, Ontario, Canada M5G 1L6 [4]Structural Biology Center, Argonne National Laboratory, Argonne, IL 60439, USA [5]York Structural Biology Laboratory, Department of Chemistry, University of York, UK [6]Structural Studies Division, MRC Laboratory of Molecular Biology, Cambridge, CB2 0QH UK [7]Midwest Center for Structural Genomics

Summary

Dethiobiotin synthetase (DTBS) is involved in the biosynthesis of biotin in bacteria, fungi and plants. As humans lack this pathway, dethiobiotin synthetase is a promising antimicrobial drug target. We determined structures of DBTS from *H. pylori* (hpDTBS) bound with cofactors and a substrate analog and described its unique characteristics relative to other DTBS proteins. Comparison with bacterial DTBS orthologues revealed considerable structural differences in nucleotide recognition. The C-terminal region of DTBS proteins, which contains two nucleotide-recognition motifs, greatly differs among DTBS proteins from different species. The structure of hpDTBS revealed that this protein is unique and does not contain a C-terminal region containing one of the motifs. The single nucleotide-binding motif in hpDTBS is similar to its counterpart in GTPases, however, ITC binding studies show that hpDTBS has a strong preference for ATP. The structural determinants of ATP specificity were assessed through X-ray crystallographic studies of hpDTBS:ATP and hpDTBS:GTP complexes. The unique mode of nucleotide recognition in hpDTBS makes this protein a good target for *H. pylori*-specific inhibitors of the biotin synthesis pathway.

Introduction

Biotin, a colorless water-soluble B-complex vitamin also known as vitamin H or vitamin B7, comprises two fused rings: an imidazole (ureido) and a sulfur-containing (tetrahydrothiophene) ring. Biotin is covalently bound to various carboxylases involved in in gluconeogenesis, fatty acid synthesis and branched chain amino acid catabolism [1]. It is also believed to play an important role in cell signaling, gene regulation, and the structure of chromatin [2].

*corresponding author: W. Minor, wladek@iwonka.med.virginia.edu.

Coordinates and structure factors for structures presented in this paper were deposited to the Protein Data Bank under following accession codes: 2QMO - *apo*-form, 3MLE – hpDTBS:8-ac:ADP:PO_4^{3-} in $P2_12_12_1$ form, 3QXC – hpDTBS:ATP, 3QXH – hpDTBS: 8-ac:ADP:PO_4^{3-} in C2 form, 3QXJ – hpDTBS:GTP, 3QXS – hpDTBS:ANP, 3QXX – 8-ac:GDP: PO_4^{3-}, and 3QY0 – hpDTBS:GDP: PO_4^{3-}.

De novo biotin synthesis occurs in *Bacteria*, *Archaea* and some *Eukaryota* (in plants and fungi) but not in animals. Biotin is thus an essential nutrient for humans, provided by intestinal flora and diet. The requirement for biotin as a vitamin and as a biotechnology reagent [3] has made biotin synthesis a process of industrial importance, and has spurred effort to improve chemical synthesis methods and biotin-overproducing organisms [1].

Because of its importance, the genetic, biochemical, and structural aspects of the biotin synthesis pathway have been intensively studied. The structures of the final four enzymes in this pathway in *E. coli* have been solved [4, 5]. These steps are conserved for all species that synthesize biotin: (a) formation of 8-amino-7-oxopelargonic acid (KAPA) from pimeloyl-CoA and alanine; (b) amination of KAPA; (c) carboxylation of diaminopelargonic acid (DAPA) and formation of the ureido ring; and (d) sulfur incorporation (Supplementary Figure 1A).

In this study, we present structures of the dethiobiotin synthetase (DTBS) from *H. pylori* (hpDTBS). Dethiobiotin synthetase (EC 6.3.3.3) catalyzes the penultimate step in biotin synthesis – the formation of the ureido ring of dethiobiotin (Supplementary Figure 1B). It has been established that CO_2 (but not HCO_3^-) and adenosine-5′-triphosphate (ATP) are needed for the carbamylation of DAPA and ring closure [6]. Two intermediates are believed to form during the reaction, the first being N7-DAPA carbamate [7-10]. In the subsequent step, carbamylated DAPA is phosphorylated with ATP and forms a second intermediate, a carbamic–phosphoric acid anhydride [11, 12]. The final step in the reaction is the closure of the ureido ring by bond formation between the N8 nitrogen and the carbonyl oxygen, and liberation of the free phosphate.

Previous analyses of ecDTBS, which utilizes ATP [6], have shown that its fold [13] and nucleotide binding mode [10] are more similar to those of GTP-binding proteins such as H-ras p21 than ATP-dependent proteins such as adenylate kinase. The similarity to GTP-binding proteins is also seen in hpDTBS, which contains a (N-L-K-G-N) motif similar to the [NQ]-[KR]-x-[DE] GTP specificity motif. It has been suggested that the first asparagine in this motif is an evolutionary relic of a protein able to bind both adenosine and guanine nucleotides [14]. Because this motif is the only fragment of hpDTBS capable of providing nucleotide specificity, investigation of the interactions of this motif with nucleotides is crucial for understanding the nucleotide preference of hpDTBS.

Here, we present eight hpDTBS structures that were determined as part of the PSI-2 Midwest Center for Structural Genomics (MCSG) effort [15]. We compare these structures with DTBS proteins from *E. coli* (ecDTBS), *M. tuberculosis* (mtDTBS) and *F. tularensis* (ftDTBS). Additionally we show that the basis of nucleotide discrimination of hpDTBS is determined by a limited set of structural features.

Results and discussion

Overall structure

hpDTBS crystallized in the *C*2 space group with one monomer in the asymmetric unit (AU) (**2QMO**, **3QXC**, **3QXH**, **3QXJ**, **3QXS**, **3QXX**, **3QY0**) and in $P2_12_12_1$ (**3MLE**) with three dimers in the AU. Crystallization conditions are presented in Table 1. The hpDTBS fold (Figure 1) is almost identical to those of ecDTBS [13, 16], mtDTBS [17] and ftDTBS (PDB code **3OF5**) (Figures 2 and 3); namely an α/β fold containing a seven-stranded parallel β-sheet surrounded by seven helices. This fold is shared with the other phosphate-binding loop (P-loop) NTPases [13, 18]. Like all other DTBS proteins with structures determined to date, hpDTBS crystallizes as a dimer, which was supported by size exclusion chromatography (data not shown). Two specific regions of the dimerization interface can be identified: (a) a

highly conserved core, formed between the P-loop and Walker B region in one subunit and the DAPA binding region in the other, and (b) a region with variable sequence but conserved structure, formed between the α3a helix of one subunit and α6 in the other, where hydrophobic interactions prevail (Figure 4).

The main difference between the folds of hpDTBS, ecDTBS and mtDTBS occurs after strand β7, where hpDTBS is missing the C-terminus fragment present in both ecDTBS and mtDTBS and partially in ftDTBS (Figures 2 and 3). This region is of functional importance to ecDTBS [10] and mtDTBS [17], where it contributes most of the binding surface for the nucleoside, including the adenine ring (Supplemental Figure 2).

Ligand binding

8-aminocaprylic acid—The lack of an amino group at position 7 (Supplemental Figures 3A and 3B) makes 8-aminocaprylic acid (8-ac) a non-reactive analog of DAPA [8, 10, 19]. The 8-ac is well ordered only in structures with a bound free phosphate group (**3QXH**, **3QXX**). The displacement of the position of the free phosphate as compared with that of the terminal NTP phosphate allowed for formation of an additional hydrogen bond between 8-ac and PO_4^{3-}. Due to a missing N7 group compared with DAPA, more than half of the hydrogen bonds stabilizing the diamino end of the bound DAPA are missing, thus, it is not surprising that 8-ac is disordered when not additionally stabilized by the free phosphate. The 8-ac:PO_4^{3-} complex resembles a phosphate anhydrite intermediate, and the complex DTB:PO_4^{3-} observed in both ecDTBS and mtDTBS. The 8-ac is found in a cavity formed by the dimerization interface near residues 8, 9, 39, 79-81, 118, 119 and 123 from the first subunit and 150-154 from the second subunit. The carboxyl group of 8-ac is hydrogen bonded by main chain amides from Gly151′, Leu152′, Ile153′ and Asn154′ (using a prime to identify residues from the opposite subunit), and bonded via water molecules by Asn8 and Ser187′ (Figure 5a). The binding mode of the 8-ac carboxyl group is essentially identical to that observed for the structures of other carboxyacids bound in other DTBS structures [10, 17] (Figure 5b). Gly151 is conserved in all DTBS proteins, Asn154 is conserved in at least 80%, and Ile153 is most commonly replaced by other hydrophobic residues (Figure 6). The amino group from 8-ac can form a hydrogen bond with the free phosphate group, and forms a water bridge to Thr39. The alkyl chain and carboxyl of 8-ac is additionally stabilized by hydrophobic interactions with Thr9, Ser79, Ala80, Pro81, Ala118, Gly119, Val123, Leu150′ and Ile153′. Analysis of the conservation of these residues suggests that they can be divided into three groups: (a) a conserved L-G-X-X-N motif binding the carboxyl end of DAPA; (b) conserved residues in the P-loop and Walker B regions forming H-bonds with the diamino-end (Thr9) or a hydrophobic pocket (Ala118, Gly119); and (c) residues present in the structurally conserved α3a helix forming a hydrophobic pocket (Figure 6).

Nucleotides and magnesium ions—The nucleotide-binding site consists of two regions, one involved in binding phosphate, and the other in binding a nucleoside. The binding mode of polyphosphate moieties in hpDTBS is the same regardless of the nucleotide (ATP – **3QXC**, ANP – **3QXS**, ADP – **3QXH**, GTP – **3QXJ** or GDP – **3QXX**, **3QY0**). The binding of triphosphates involves residues 9, 10, 12-15, 50 and 116, whereas the binding of the free phosphate presumably liberated during the reaction or incorporated from solution additionally involves the Lys35 and Gly119 residues.

All of the phosphate binding residues can be divided into three groups: a Walker A motif, a Walker B motif and a region conserved in DTBS proteins but not other nucleoside triphosphatases (NTPases) from different families [18]. Residues belonging to the Walker A motif form a P-loop between α1 and β1, and interact with phosphates by their side chains (Thr9, Lys13, Thr14, Thr15) and/or main chain amides (Asn10, Gly12, Lys13, Thr14,

Thr15). They are characterized by high conservation amongst P-loop containing NTPases. However, the P-loop in DTBSes contains additional threonine (Thr9 in hpDTBS), that has been found to form a hydrogen bond with DAPA-N8 in ecDTBS [9], while it forms only hydrophobic interactions with the 8-ac aliphatic chain in hpDTBS:8-ac:NDP:PO_4^{3-} (**3QXH**, **3QXX**) complexes. The second phosphate binding region includes residues from the Walker B motif, Glu116 and Gly119, which bind phosphates by the side chain and main chain amide, respectively. Gly119 is involved only in the binding of the free phosphate group. The third group consists of fully conserved amino acids present only in DTBS proteins [18]. Lys35 binds a free phosphate and is considered a main catalytic residue [20], and Asp50 is not only involved in the binding of phosphates but also coordinates a magnesium ion.

By comparing the structures of DTBS proteins from four different species, it becomes apparent that the only differences in the binding mode of phosphates observed between them are in two positions: hpDTBS Thr15 (corresponding to ecDTBS Val15, mtDTBS Val17, and ftDTBS Tyr17) and hpDTBS Asn10 (corresponding to ecDTBS Glu12, mtDTBS Gly12, and ftDTBS Glu12). For ATP binding, the replacement of Val with Thr allows the formation of an additional hydrogen bond between the side chain of Thr15 and the α-phosphate group. Tyr17 in ftDTBS is also in an appropriate position to form a π – π stacking interaction with the adenine ring. Glu to Asn substitution prevents the direct binding of the β- and γ-phosphates, which is facilitated through a water molecule. These two residues seem to be nonessential for phosphate binding, as suggested by the low degree of conservation in these two positions (Figures 6 and 7) and supported by mutagenesis studies [20].

The other residues observed to bind the phosphate moieties of nucleotides, some of which are characteristic for P-loop-containing NTPases [14, 18] and others which are unique to DTBS proteins (Lys35 and Asp50) are highly conserved both in sequence and structure. The role of Asp50 has not been previously investigated; its interaction with Lys35 suggests that it may be responsible for stabilizing this catalytically active lysine residue. Interestingly, Asp50 is located in a region between the C-terminus ends of the β2 and β3 strands, which appears to be highly structurally conserved among DTBS structures, despite relatively low sequence conservation. Asp50 also coordinates a conserved magnesium ion, but there is no corresponding residue on the surface motif of P-loop NTPases [14].

All structures of hpDTBS complexed with nucleotides (**3MLE**, **3QXC**, **3QXH**, **3QXJ**, **3QXS**, **3QXX**, **3QY0**) contain at least one magnesium ion coordinated by residues Thr15, Asp50 and Glu116 and the β- and γ-phosphates of NTPs, or by the β-phosphate of NDP and a free phosphate group. The position of this ion is conserved among all P-loop NTPases [14]. A second magnesium ion was identified in the structures of the diphosphate forms (**3QXH**, **3QXX**, **3QY0**; with the exception of the **3MLE** - most probably due to the lower resolution of this crystal form) and is coordinated by the free phosphate, the β-phosphate of NDP, and waters bound by conserved residues Thr9, Asp10 and Glu116. Two magnesium ions were previously observed in ecDTBS as well [21]. It was suggested that the second magnesium ion not only stabilizes the reaction intermediate [21], but also acts as the conserved positive charge required for ATP hydrolysis [14].

Nucleoside recognition—The spatial arrangement of amino acids in the nucleotide binding pocket of the nucleotide-bound hpDTBS structures is very similar to the H-ras p21:GNP complex (Figure 8). We therefore conducted an ITC experiment to determine nucleotide specificity and calculated binding parameters of various nucleotides. ATP and ADP have dissociation constants of 1.7 μM and 5.8 μM, respectively (Supplemental Figure 4), but binding of GDP or GTP was not detected under the same conditions. To investigate why the hpDTBS resembles GTP-binding proteins but preferentially binds ATP, we

crystallized complexes of hpDTBS together with GTP and GDP and compared the nucleotide binding in hpDTBS, ecDTBS and H-ras p21.

The nucleoside moieties of the nucleotides have different binding modes for adenosine (**3MLE**, **3QXC**, **3QXH**, **3QXS**) versus guanosine nucleotides (**3QXX**) (Figure 8). The adenine moiety is bound by Asn175 via two hydrogen bonds. The ribose of adenosine nucleotides is bound through two water molecules: one bound to Thr15 and the other to Asp10 and Lys177. Additionally, Thr15 and Lys177 stabilize the purine rings of both adenine and guanine moieties by hydrophobic interactions. The main chain atoms of Leu176 and Gly178 bind adenine through water molecules. Additional (most likely non-physiological) interactions with Gln167 (in monoclinic crystal forms) and Arg63 (in the 3MLE structure) are introduced by crystallization of hpDTBS. As mentioned above, hpDTBS lacks the C terminus that interacts with the nucleoside and contains the adenosine specificity motif [22]; thus the specific interactions between ecDTBS and adenosine are not present in hpDTBS. For example, in the equivalent positions of H-bonds with the main chain amides of Pro204 and Leu206 in ecDTBS H-bonds formed between waters and adenine are found in the hpDTBS models.

The position of the guanine moiety of a guanosine nucleotide could be unambiguously determined only in the hpDTBS:GDP:PO_4^{3-} (**3QXX**) complex. In this structure, the guanine makes a single hydrogen bond to Asn175. Water molecules bridge guanine and the side chain of Asp175 and main chain atoms of Leu176 and Gly178. The guanine is also most likely stabilized by hydrophobic interactions with the Lys177 side chain. hpDTBS does not form most of the interactions that are formed between H-ras p21 and guanine moiety. In particular, there are no interactions equivalent to the H-bonds formed between H-ras p21 Asp119 and Ala146 and guanine. Furthermore, the hydrophobic interactions provided by H-ras p21 Phe28 and Lys147 are missing in hpDTBS. In addition, hpDTBS Asn175 assumes a different orientation with respect to the guanine ring that is observed for H-ras p21 Asn116 and forms an additional water bridge with purine ring.

The only difference observed between ADP and GDP binding in hpDTBS is that there is only one hydrogen bond formed between Asn175 and guanosine, whereas two are present for adenine. The lack of the second strong hydrogen bond may explain the higher disorder observed for bound GDP and the stronger binding of ATP as shown by ITC experiments. However, we cannot rule out the effect of presumably non-physiological interactions present between nucleoside groups and symmetry-related subunits of hpDTBS on the binding mode of GDP.

Conclusions

Determination of several structures of hpDTBS in complex with a number of cofactors and substrate analogs allowed us to correlate features of the observed binding sites with bioinformatic analysis of different DTBS proteins. Despite relatively low overall sequence identity, hpDTBS is structurally very similar to other DTBSes and share a fold in common with P-loop NTPases. Moreover, the catalytic site in htDTBS is highly conserved in terms of sequence (Figure 6) and structure (Figure 7) amongst bacterial and archaeal species. The observed modes of ligand binding are virtually the same to those observed for ecDTBS and mtDTBS.

The main differences between DTBS proteins can be found around the C-terminus where sequence analysis showed large degree of variability. This region appears to carry two motifs responsible for nucleotide recognition. One motif related to the guanosine recognition region in GTPases is located in the sequence immediately after the conserved β6 strand. A

second motif which may be associated with the adenosine recognition region in ATPases is formed on a C-terminal flexible loop. The structures of hpDTBS revealed that this protein is unique among DTBS proteins of known structure, as it does not contain the second C-terminal motif. Moreover hpDTBS also lacks structural elements analogous to those responsible for GTP recognition in H-ras p21. Our binding study showed that hpDTBS is able to effectively recognize ATP, despite lacking most of the structural specificity determinants seen in other DTBS proteins. Asn175, which was previously thought to be an evolutionary relic [14], mediates all the specific interactions with the adenine moiety.

Interestingly, previous studies on mtDTBS showed that the changes in the composition and conformation of the nucleotide recognizing motifs (relative to ecDTBS) change the kinetic characteristics of the protein, which may have an influence on an organism's pathogenicity [17]. A lead compound targeting the adenine recognition site of ecDTBS has been designed [23]. Further developments may lead to the production of good inhibitors and specific drugs targeting hpDTBS.

Experimental procedures

Protein cloning, expression and purification

The *hp0029* gene (MCSG target APC5858) was cloned using the standard protocol developed at the MCSG, as described previously [24]. The native protein was obtained as follows: a construct of *hp0029* in the p11 vector was transformed into *E. coli* strain BL21-Gold(DE3)Magic, which harbors an extra plasmid encoding three rare tRNAs (AGG and AGA for Arg; and ATA for Ile). Cells were grown in 1 L flasks of LB medium at 37°C until the optical density at 600 nm reached ~0.6. After induction with isopropyl-1-β-D-thiogalactopyranoside to a final concentration of 0.5 mM, cells were incubated with shaking overnight at 20°C. Harvested cells were resuspended in a binding buffer containing 500 mM NaCl, 50 mM HEPES pH 7.5, 5% glycerol, 5 mM imidazole, 1 mM phenylmethanesulfonylfluoride and 1 mM benzamidine. After sonication the lysate was clarified by centrifugation and the supernatant was applied to a nickel chelate affinity resin (Ni–NTA, Qiagen) previously equilibrated with binding buffer (the resuspension buffer minus the protease inhibitors). Next, the resin was washed with washing buffer (500 mM NaCl, 50 mM HEPES pH 7.5, 5% glycerol, 30 mM imidazole), and the protein was eluted with elution buffer (500 mM NaCl, 5% glycerol, 50 mM HEPES pH 7.5, and 250 mM imidazole). Protein was then concentrated and purified further using a gel filtration column (HiLoad 6/16 Superdex 200) on an AKTA FPLC system (GE Healthcare) with buffer containg 500 mM NaCl and 10 mM HEPES pH 7.5. After purification, protein was concentrated to 27 mg/mL using Amicon (Millipore) centrifugal filter units with a 10kDa molecular weight cut-off.

Selenomethionine derivatives of hpDTBS were expressed and purified as described previously [25].

Crystallization

The crystallization of a selenomethionine derivative of hpDTBS was performed using *in situ* proteolysis as described by Dong and coworkers [25]. 1 mg of chymotrypsin per 100 mg of protein was added to each of the crystallization drops. Detailed crystallization and soaking conditions for each of the obtained structures are presented in Table 1 (see Supplementary Methods for crystallization and soaking procedures). Generation of an optimization strategy, crystal and drop tracking and analysis of intermediate results were performed using the crystallization database Xtaldb [26, 27]. Crystals were harvested using CryoLoops from

Hampton Research, immediately transferred into cryoprotectant solution containing a 2:1 mixture of mother liquor and ethylene glycol and flash-cooled in liquid nitrogen.

Data collection, structure solution and refinement

Diffraction data were collected at a temperature of 100 K at beamlines 19-BM and 19-ID of the Structural Biology Center at the Advanced Photon Source (APS) [28]. Data collection, structure determination, and refinement statistics are summarized in Table 2. Data were processed with HKL-2000 [29] and HKL-3000 [30]. The structure of the *apo*-form of hpDTBS was solved by Se single-wavelength anomalous diffraction (SAD). Phasing and initial models were performed with HKL-3000, integrated with SHELXD, SHELXE [31], MLPHARE [32], DM [33], ARP/wARP [34], SOLVE [35] and RESOLVE [36, 37]. The resultant model was further refined with REFMAC5 [38] and COOT [39]. All other structures were solved by molecular replacement (MR) using the 2QMO model, as implemented in HKL-3000 coupled with MOLREP [40] and refined with REFMAC5 and COOT. The TLSMD server was used for identification of optimal TLS groups [41, 42]. MOLPROBITY [43] and ADIT [44] were used for structure validation.

Structural alignment of E. coli and H. pylori DTBSes

Models of *apo*-forms of DTBS proteins were aligned with the following structures: **1BYI** for ecDTBS, **2QMO** for hpDTBS, **3FGN** for mtDTBS, and **3OL5** for ftDTBS. Structure-based pairwise sequence alignments from DaliLite [45] and a multiple alignment from SSM [46] were combined. The sequence alignments obtained from the servers were used to superpose the structures by minimizing the distances between C_α atoms of corresponding residues using least-squares methods. The fragments of the sequence alignments that yielded the best local superposition in terms of distance between corresponding C_α were combined. Finally, the superposed structures were inspected, minor manual alterations to the alignments were introduced, and the superposition recalculated using only corresponding residues that aligned with inter-C_α distances lower than 1 Å. Thus obtained structural alignment of the *apo*-forms was used for calculating all superpositions of the corresponding complexes of ecDTBS, hpDTBS, mtDTBS and ftDTBS.

Multiple sequence alignment of DTBSes

The sequence of hpDTBS was used to perform a PSI-BLAST [47] search against the non-redundant subset of the NCBI protein sequence database (28 Feb 2011) using the procedure described in Supplementary Methods

The structural alignment of hpDTBS, ecDTBS, mtDTBS and ftDTBS showed that the secondary structure elements are highly conserved despite low sequence similarity. The PROMALS3D server [48, 49] was used to calculate the multiple sequence alignment (MSA) of the non-redundant sequences using constraints derived from the structural alignment. The MSA was then manually refined. Consensus sequences were calculated using tools from the http://coot.embl.de/Alignment/ website. The AL2CO server [50] was used to calculate the positional conservation of the non-redundant set of sequences.

Isothermal titration calorimetry (ITC)

ITC measurements were performed at 25 °C using an iTC200 isothermal titration calorimeter (MicroCal). Protein preparations were dialyzed against a 100 mM HEPES-Na pH 7.5 buffer and diluted to a final hpDTBS concentration of 36 μM. All cofactors were dissolved in the same buffer. The protein was titrated with 26 injections of either 540 μM ATP, 700 μM ADP or 700 μM GDP. The first injection of each cofactor solution had a volume of 0.5 μL, followed by twenty-five 1.5 μL injections at 180 s intervals. Since

binding of GDP was not observed, 1 mM of GTP was used to titrate the same sample after all GDP injections.

Supplementary Material

Refer to Web version on PubMed Central for supplementary material.

Acknowledgments

The authors would like thank Dr. Matthew D. Zimmerman for valuable discussions. We thank Dr. Igor Shumilin for help with ITC experiments. The work described in the paper was supported by NIH PSI grant GM074942.

The results shown in this report are derived from work performed at Argonne National Laboratory, at the Structural Biology Center of the Advanced Photon Source. Argonne is operated by the University of Chicago Argonne, LLC, for the U.S. Department of Energy, Office of Biological and Environmental Research, under contract DE-AC02-06CH11357.

References

1. Streit WR, Entcheva P. Biotin in microbes, the genes involved in its biosynthesis, its biochemical role and perspectives for biotechnological production. Appl Microbiol Biotechnol. 2003; 61:21–31. [PubMed: 12658511]
2. Zempleni J. Uptake, localization, and noncarboxylase roles of biotin. Annu Rev Nutr. 2005; 25:175–96. [PubMed: 16011464]
3. Laitinen OH, Nordlund HR, Hytonen VP, Kulomaa MS. Brave new (strept)avidins in biotechnology. Trends Biotechnol. 2007; 25:269–77. [PubMed: 17433846]
4. Berkovitch F, Nicolet Y, Wan JT, Jarrett JT, Drennan CL. Crystal structure of biotin synthase, an S-adenosylmethionine-dependent radical enzyme. Science. 2004; 303:76–9. [PubMed: 14704425]
5. Schneider G, Lindqvist Y. Structural enzymology of biotin biosynthesis. FEBS Lett. 2001; 495:7–11. [PubMed: 11322938]
6. Krell K, Eisenberg MA. The purification and properties of dethiobiotin synthetase. J Biol Chem. 1970; 245:6558–66. [PubMed: 4921568]
7. Baxter RL, Ramsey AJ, Mciver LA, Baxter HC. Mechanism of Dethiobiotin Synthetase - Characterization of the 8-Aminocarbamate of (7r,8s)-7,8 Diaminononanoate as an Enzyme-Bound Intermediate. J Chem Soc Chem Comm. 1994:559–560.
8. Gibson KJ, Lorimer GH, Rendina AR, Taylor WS, Cohen G, Gatenby AA, Payne WG, Roe DC, Lockett BA, Nudelman A, Marcovici D, Nachum A, Wexler BA, Marsilii EL, Turner IM, Howe LD, Kalbach CE, Chi HJ. Dethiobiotin Synthetase - the Carbonylation of 7,8-Diaminononanoic Acid Proceeds Regiospecifically Via the N7-Carbamate. Biochemistry. 1995; 34:10976–10984. [PubMed: 7669755]
9. Alexeev D, Baxter RL, Smekal O, Sawyer L. Substrate-Binding and Carboxylation by Dethiobiotin Synthetase - a Kinetic and X-Ray Study. Structure. 1995; 3:1207–1215. [PubMed: 8591031]
10. Huang WJ, Jia J, Gibson KJ, Taylor WS, Rendina AR, Schneider G, Lindqvist Y. Mechanism of an Atp-Dependent Carboxylase, Dethiobiotin Synthetase, Based on Crystallographic Studies of Complexes with Substrates and a Reaction Intermediate. Biochemistry. 1995; 34:10985–10995. [PubMed: 7669756]
11. Baxter RL, Baxter HC. The Mechanism of Escherichia-Coli Dethiobiotin Synthetase - the Closure of the Ureido Ring of Dethiobiotin Involves Formation of a Carbamic-Phosphate Mixed Anhydride. J Chem Soc Chem Comm. 1994:759–760.
12. Gibson KJ. Isolation and chemistry of the mixed anhydride intermediate in the reaction catalyzed by dethiobiotin synthetase. Biochemistry. 1997; 36:8474–8478. [PubMed: 9214291]
13. Huang WJ, Lindqvist Y, Schneider G, Gibson KJ, Flint D, Lorimer G. Crystal-Structure of an Atp-Dependent Carboxylase, Dethiobiotin Synthetase, at 1.65-Angstrom Resolution. Structure. 1994; 2:407–414. [PubMed: 8081756]

14. Via A, Ferre F, Brannetti B, Valencia A, Helmer-Citterich M. Three-dimensional view of the surface motif associated with the P-loop structure: Cis and trans cases of convergent evolution. Journal of Molecular Biology. 2000; 303:455–465. [PubMed: 11054283]
15. Grabowski M, Joachimiak A, Otwinowski Z, Minor W. Structural genomics: keeping up with expanding knowledge of the protein universe. Curr Opin Struc Biol. 2007; 17:347–353.
16. Alexeev D, Baxter RL, Sawyer L. Mechanistic Implications and Family Relationships from the Structure of Dethiobiotin Synthetase. Structure. 1994; 2:1061–1072. [PubMed: 7881906]
17. Dey S, Lane JM, Lee RE, Rubin EJ, Sacchettini JC. Structural characterization of the Mycobacterium tuberculosis biotin biosynthesis enzymes 7,8-diaminopelargonic acid synthase and dethiobiotin synthetase. Biochemistry. 2010; 49:6746–60. [PubMed: 20565114]
18. Leipe DD, Wolf YI, Koonin EV, Aravind L. Classification and evolution of P-loop GTPases and related ATPases. Journal of Molecular Biology. 2002; 317:41–72. [PubMed: 11916378]
19. Rendina AR, Taylor WS, Gibson K, Lorimer G, Rayner D, Lockett B, Kranis K, Wexler B, Marcovici-Mizrahi D, Nudelman A, Nudelman A, Marsilii E, Chi HJ, Wawrzak Z, Calabrese J, Huang WJ, Jia J, Schneider G, Lindqvist Y, Yang G. The design and synthesis of inhibitors of dethiobiotin synthetase as potential herbicides. Pestic Sci. 1999; 55:236–247.
20. Yang G, Sandalova T, Lohman K, Lindqvist Y, Rendina AR. Active site mutants of Escherichia coli dethiobiotin synthetase: Effects of mutations on enzyme catalytic and structural properties. Biochemistry. 1997; 36:4751–4760. [PubMed: 9125495]
21. Kack H, Sandmark J, Gibson KJ, Schneider G, Lindqvist Y. Crystal structure of two quaternary complexes of dethiobiotin synthetase, enzyme-MgADP-AlF3-diaminopelargonic acid and enzyme-MgADP-dethiobiotin-phosphate; implications for catalysis. Protein Sci. 1998; 7:2560–2566. [PubMed: 9865950]
22. Denessiouk KA, Johnson MS. When fold is not important: A common structural framework for adenine and AMP binding in 12 unrelated protein families. Proteins. 2000; 38:310–326. [PubMed: 10713991]
23. Alexeev D, Baxter RL, Campopiano DJ, McAlpine RS, McIver L, Sawyer L. Rational design of an inhibitor of dethiobiotin synthetase; Interaction of 6-hydroxypyrimidin-4(3H)-one with the adenine base binding site. Tetrahedron. 1998; 54:15891–15898.
24. Zhang RG, Skarina T, Katz JE, Beasley S, Khachatryan A, Vyas S, Arrowsmith CH, Clarke S, Edwards A, Joachimiak A, Savchenko A. Structure of Thermotoga maritima stationary phase survival protein SurE: A novel acid phosphatase. Structure. 2001; 9:1095–1106. [PubMed: 11709173]
25. Dong AP, Xu XH, Edward AM. Mcsg&Sgc. In situ proteolysis for protein crystallization and structure determination. Nat Methods. 2007; 4:1019–1021. [PubMed: 17982461]
26. Zimmerman M, Chruszcz M, Koclega K, Otwinowski Z, Minor W. The Xtaldb system for project salvaging in high-throughput crystallization. Acta Crystallographica Section A. 2005; 61:c178–c179.
27. Cymborowski M, Klimecka M, Chruszcz M, Zimmerman MD, Shumilin IA, Borek D, Lazarski K, Joachimiak A, Otwinowski Z, Anderson W, Minor W. To automate or not to automate: this is the question. J Struct Funct Genomics. 2010; 11:211–21. [PubMed: 20526815]
28. Rosenbaum G, Alkire RW, Evans G, Rotella FJ, Lazarski K, Zhang RG, Ginell SL, Duke N, Naday I, Lazarz J, Molitsky MJ, Keefe L, Gonczy J, Rock L, Sanishvili R, Walsh MA, Westbrook E, Joachimiak A. The Structural Biology Center 19ID undulator beamline: facility specifications and protein crystallographic results. J Synchrotron Radiat. 2006; 13:30–45. [PubMed: 16371706]
29. Otwinowski Z, Minor W. Processing of X-ray diffraction data collected in oscillation mode. Method Enzymol. 1997; 276:307–326.
30. Minor W, Cymborowski M, Otwinowski Z, Chruszcz M. HKL-3000: the integration of data reduction and structure solution - from diffraction images to an initial model in minutes. Acta Crystallogr D. 2006; 62:859–866. [PubMed: 16855301]
31. Sheldrick GM. A short history of SHELX. Acta Crystallographica Section A. 2008; 64:112–122.
32. Otwinowski, Z. Isomorphous Replacement and Anomalous Scattering. Paper presented at the Daresbury Study Weekend Proceedings, SERC Daresbury Laboratory; Warrington, U.K. 1991.

33. Cowtan KD, Main P. Improvement of Macromolecular Electron-Density Maps by the Simultaneous Application of Real and Reciprocal Space Constraints. Acta Crystallogr D. 1993; 49:148–157. [PubMed: 15299555]
34. Perrakis A, Morris R, Lamzin VS. Automated protein model building combined with iterative structure refinement. Nat Struct Biol. 1999; 6:458–463. [PubMed: 10331874]
35. Terwilliger TC, Berendzen J. Automated MAD and MIR structure solution. Acta Crystallogr D. 1999; 55:849–861. [PubMed: 10089316]
36. Terwilliger TC. Automated structure solution, density modification and model building. Acta Crystallogr D. 2002; 58:1937–1940. [PubMed: 12393925]
37. Terwilliger T. SOLVE and RESOLVE: automated structure solution, density modification, and model building. J Synchrotron Radiat. 2004; 11:49–52. [PubMed: 14646132]
38. Murshudov GN, Skubak P, Lebedev AA, Pannu NS, Steiner RA, Nicholls RA, Winn MD, Long F, Vagin AA. REFMAC5 for the refinement of macromolecular crystal structures. Acta Crystallogr D. 2011; 67:355–367. [PubMed: 21460454]
39. Emsley P, Lohkamp B, Scott WG, Cowtan K. Features and development of Coot. Acta Crystallogr D. 2010; 66:486–501. [PubMed: 20383002]
40. Vagin A, Teplyakov A. MOLREP: an automated program for molecular replacement. J Appl Crystallogr. 1997; 30:1022–1025.
41. Painter J, Merritt EA. Optimal description of a protein structure in terms of multiple groups undergoing TLS motion. Acta Crystallogr D. 2006; 62:439–450. [PubMed: 16552146]
42. Painter J, Merritt EA. TLSMD web server for the generation of multi-group TLS models. J Appl Crystallogr. 2006; 39:109–111.
43. Lovell SC, Davis IW, Adrendall WB, de Bakker PIW, Word JM, Prisant MG, Richardson JS, Richardson DC. Structure validation by C alpha geometry: phi,psi and C beta deviation. Proteins. 2003; 50:437–450. [PubMed: 12557186]
44. Yang HW, Guranovic V, Dutta S, Feng ZK, Berman HM, Westbrook JD. Automated and accurate deposition of structures solved by X-ray diffraction to the Protein Data Bank. Acta Crystallogr D. 2004; 60:1833–1839. [PubMed: 15388930]
45. Holm L, Park J. DaliLite workbench for protein structure comparison. Bioinformatics. 2000; 16:566–567. [PubMed: 10980157]
46. Krissinel E, Henrick K. Secondary-structure matching (SSM), a new tool for fast protein structure alignment in three dimensions. Acta Crystallogr D. 2004; 60:2256–2268. [PubMed: 15572779]
47. Altschul S, Madden T, Schaffer A, Zhang JH, Zhang Z, Miller W, Lipman D. Gapped BLAST and PSI-BLAST: A new generation of protein database search programs. Faseb J. 1998; 12:A1326–A1326.
48. Pei JM, Tang M, Grishin NV. PROMALS3D web server for accurate multiple protein sequence and structure alignments. Nucleic Acids Res. 2008; 36:W30–W34. [PubMed: 18503087]
49. Pei JM, Kim BH, Grishin NV. PROMALS3D: a tool for multiple protein sequence and structure alignments. Nucleic Acids Res. 2008; 36:2295–2300. [PubMed: 18287115]
50. Pei JM, Grishin NV. AL2CO: calculation of positional conservation in a protein sequence alignment. Bioinformatics. 2001; 17:700–712. [PubMed: 11524371]
51. Hutchinson EG, Thornton JM. PROMOTIF - A program to identify and analyze structural motifs in proteins. Protein Sci. 1996; 5:212–220. [PubMed: 8745398]

Abbreviations

DTBS	dethiobiotin synthetase
hpDTBS	dethiobiotin synthetase from *H. pylori*
ecDTBS	dethiobiotin synthetase from *E. coli*
mtDTBS	dethiobiotin synthetase from *M. tuberculosis*
ftDTBS	dethiobiotin synthetase from *F. tularensis*

DAPA	diaminopelargonic acid
8-ac	8-aminocaprylic acid
P-loop	phosphate-binding loop
AU	asymmetric unit
NTP	nucleotide triphosphate
ITC	isothermal titration calorimetry

Highlights

- Structures of hpDTBS and its complexes reveals cofactor and substrate binding modes
- Structure and sequence comparison of DTBS proteins shows C-terminal variability
- Lack of the second nucleotide-recognizing motif in hpDTBS does not impair ATP binding

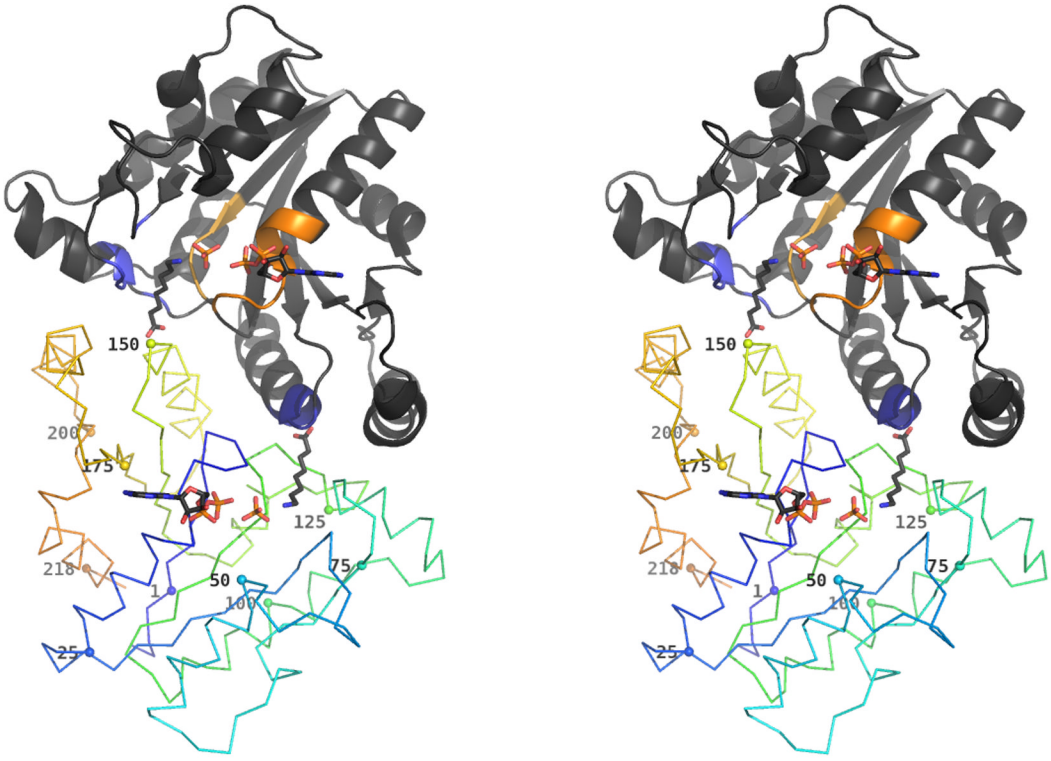

Figure 1. Overview of hpDTBS dimer with bound ADP, phosphate and 8-aminocaprylic acid

One of the monomers is rendered in cartoon representation. The colored regions of this monomer correspond to the phosphate binding region comprising the Walker A (orange) and Walker B (yellow) motifs, and the DAPA binding region with the hydrophobic pocket (light blue) and DAPA specific region (dark blue).

The other monomer is rendered as a ribbon, with and with gradually changing color from N-terminus (blue) to C-terminus (orange). The C_α atom of every 25^{th} residue is marked with a sphere and labeled with residue number.

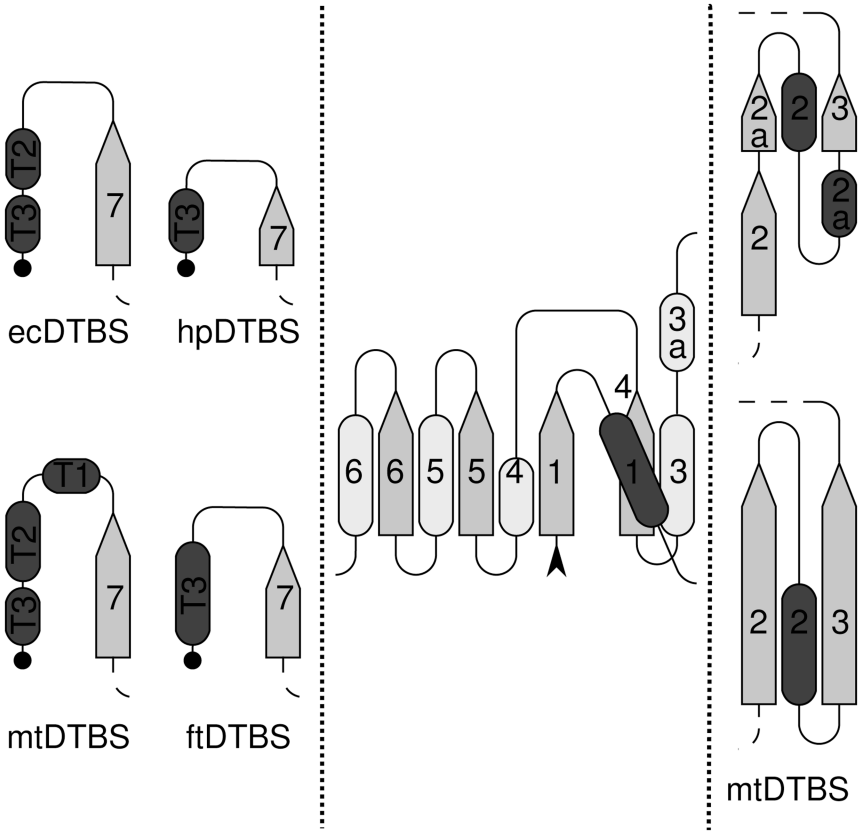

Figure 2. Topology diagram of DTBSes

β-strands are shown as arrows pointing toward the C-terminus. Helices are shown as dark rods above the plane of the β-sheet, or as light gray rods below the β-sheet. A black arrowhead marks the N-terminus of the protein, and the C-termini are depicted as black dots. The center panel shows the region common to all four structures: **1BYI** (ecDTBS), **2QMO** (hpDTBS), **3FGN** (mtDTBS) and **3OF5** (ftDTBS). The left panel displays the topological differences between the C-termini of these proteins. The right panel shows the differences in secondary structure of mtDTBS versus the other DTBS structures β-strands 2 and 3. Diagrams were prepared using the protocol of *PROMOTIF* [51] for secondary structure assignment of *apo*-forms of enzymes. The annotation of secondary structure elements is consistent with the annotation made previously for ecDTBS [13]

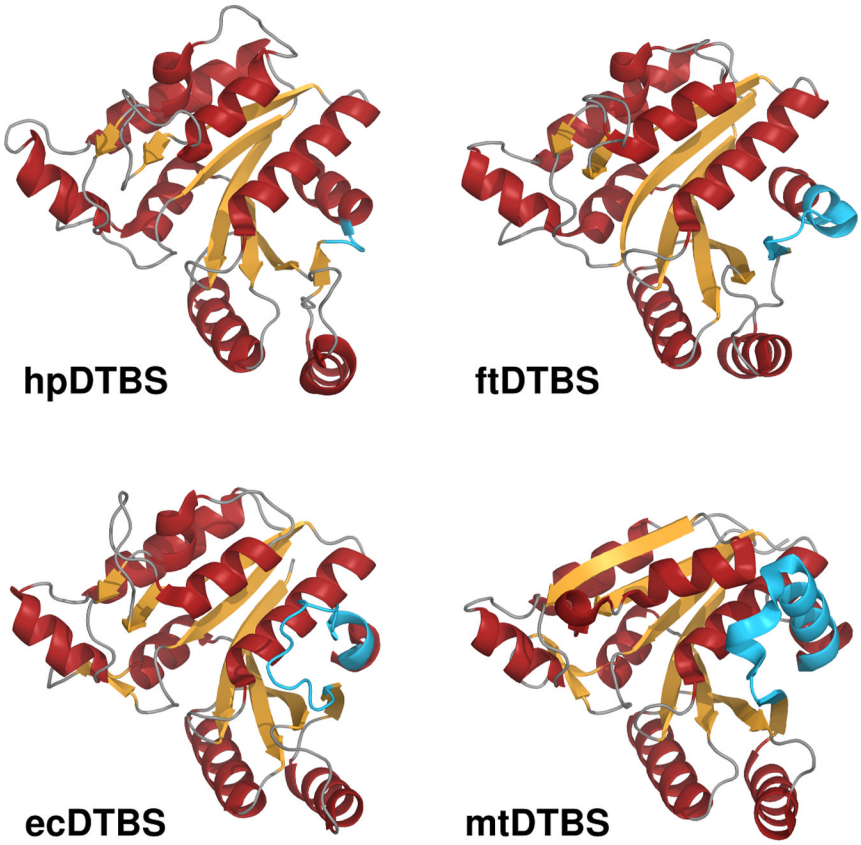

Figure 3. Overview of superposed DTBS structures

Comparison of the structures of hpDTBPS (**2QMO**), ftDTBS (**3OF5**), ecDTBS (**1BYI**) and mtDTBS (**3FGN**), in cartoon representation with α-helices rendered in red and β-strands rendered in orange. The C-terminal fragments responsible for nucleoside binding contributing to differences between these DTBSes are shown in blue. See also Figure S2 for comparison of nucleotide binding surfaces.

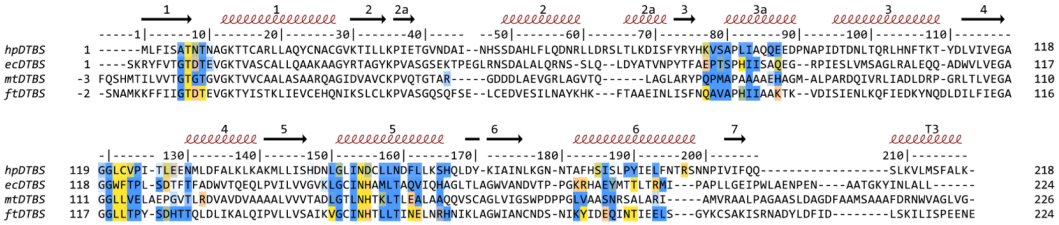

Figure 4. Structure-based sequence alignment of DTBS proteins

Residues involved in dimer formation are annotated as follows: yellow residues form hydrogen bonds, orange form salt bridges, and blue residues are involved in hydrophobic interactions. Residues in equivalent positions forming different interactions in different structures of a given protein are annotated in green (i.e. residues that form hydrogen bonds in some of the models and solely hydrophobic interactions in others). The intensity of color is proportional to the fraction of models where the given interaction occurs. Numbers on top of the alignment correspond to residue numbers from hpDTBS.

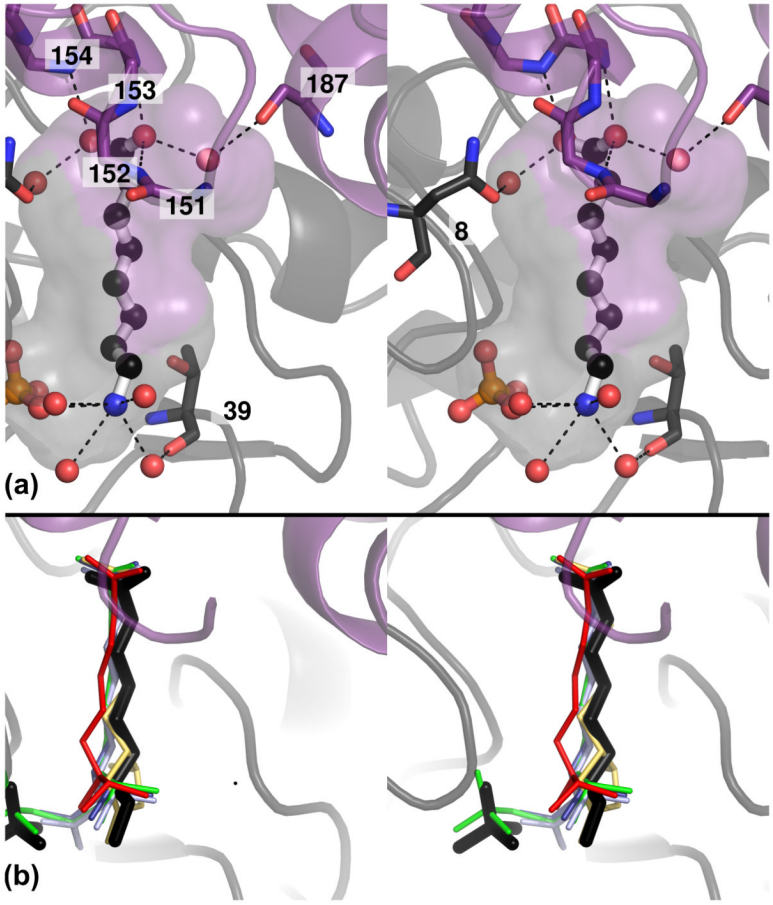

Figure 5. Substrate binding pocket of hpDTBS

A – Stereo view of the substrate binding pocket formed at the protein dimerization interface. The cavity formed by two subunits is represented as a semitransparent surface, colored either purple or gray corresponding to the monomer forming the given part of the cavity. The proteins are represented as cartoons, and residues involved in 8-ac binding are shown as sticks. Bound 8-ac and free phosphate are rendered in ball and stick representation. Dashed lines represent likely hydrogen bonds.

B – Stereo view of the substrate binding pocket with superimposed substrates, substrate analogues and reaction products and intermediates from different models of DTBS proteins: dethiobiotin in ecDTBS in yellow (**1DAM**), DAPA in ecDTBS in red (**1A82**), 7-carboxyamino-8-aminopelargonic acid in ecDTBS in blue (**1DAF**) and in mtDTBS in light blue (**3FMF**), and DAPA carbamic–phosphoric acid anhydride in ecDTBS in green (**1DAK**). See also Figure S3.

Figure 6. Representative subset of the multiple sequence alignment of DTBS proteins

Non-redundant sequences selected with a 20% identity threshold are presented together with sequences from DTBS proteins of known structure. Consensus sequences and conservation values are calculated for the complete MSA. Conservation values are coded by intensity – invariant positions are marked in black, and not conserved in gray. Residues from DTBS proteins of known structure are colored according to which binding pocket they belong: residues binding nucleotides (ecDTBS, hpDTBS) or phosphate ions (for mtDTBS) are in orange, residues binding magnesium ions in green, and residues forming binding cavity for DAPA or its analogs in blue. Color bars on top of the alignment correspond to Walker A (dark orange), Walker B (light orange) and DAPA (blue) specificity motifs. This color scheme is consistent with the color scheme used in Figure 1. Numbers on top of the alignment correspond to residue numbers from hpDTBS. Information about species origin of presented sequences is included in Supplementary Table 1.

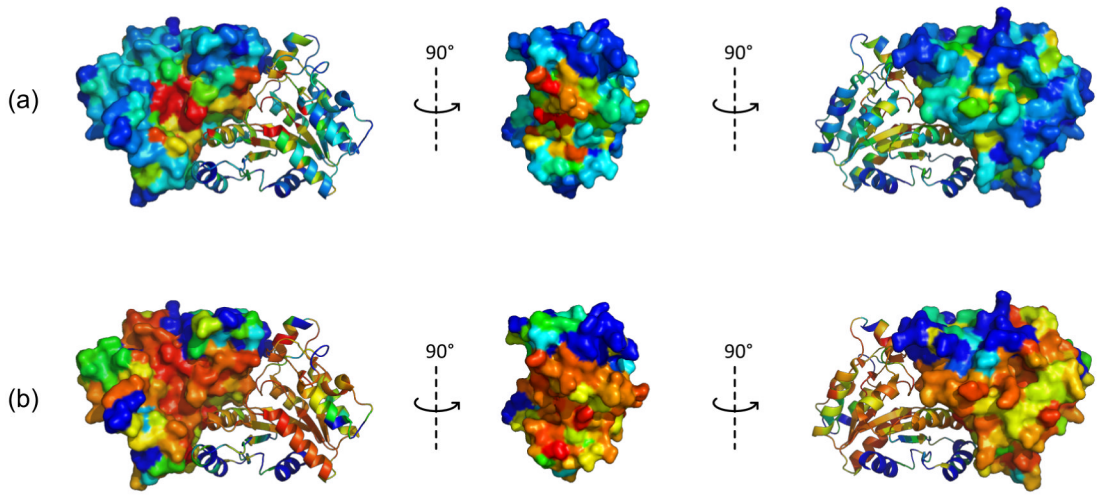

Figure 7. Sequence and structural conservation of DTBS proteins

Three different orientations of the structure of hpDTBS (**2QMO**), colored by degree of sequence or structural conservation. In each image, one monomer is shown as a cartoon and the other as a surface. (**A)** Sequence conservation of DTBS proteins in the MSA. Colors range from red for invariant residues to blue for residues for no sequence conservation. (**B)** Structural conservation as calculated by C_α distances between corresponding residues of the superimposed *apo*-structures of ecDTBS (**1BYI**) and hpDTBS (**2QMO**). Colors range from red for residues with minimal C_α distances to blue for residues with C_α distances higher than 4 Å.

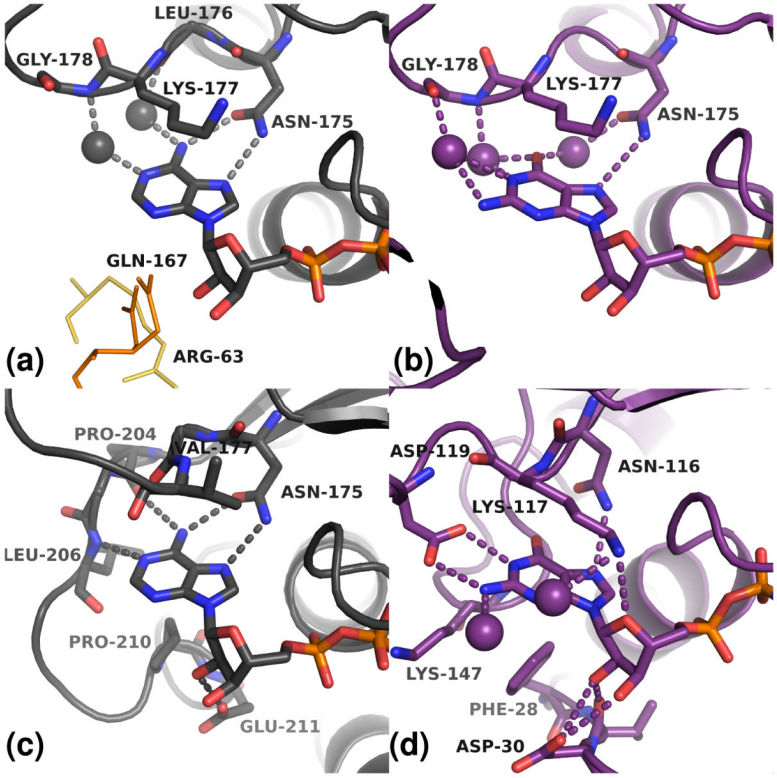

Figure 8. Nucleotide binding modes of hpDTBS compared to ecDTBS and H-ras p21

(A) the hpDTBS:ATP complex (B) hpDTBS:GDP:PO_4^{3-} complex (C) ecDTBS:ADP complex (D) H-ras p21:GNP complex. Residues involved in nucleoside binding are shown as sticks. Probable hydrogen bonds are shown as dashes. Waters involved in nucleoside binding are shown as spheres. Other symmetry-related subunits of the protein also interact with the adenosine nucleoside moiety: in the low resolution hpDTBS:8-ac:ADP: PO_4^{3-} structure as yellow lines, and in the hpDTBS:ATP structure as orange lines, see Figure S4 and main text for results of ITC binding experiment.

Table 1

Crystallization conditions that produced hpDTBS crystals

All crystals were grown in the presence of 1 mg chymotrypsin per 100 mg of protein, with 100mM Bis-Tris in pH 5.5. Detergents used (Anatrace): A - 1% w/v Anzergent 3-8; C - 1% w/v Cygent. When present, glycerol was added to a final concentration of 5% v/v. Only components additional to these in mother liquor are listed in soaking solution composition.

		Mother liquor composition					Soaking solution composition		
Complex	**PDB id**	**PEG 3350 [% w/v]**	**NH_4NO_3 [mM]**	**Detergent**	**Glycerol**	**Other**			
apo	**2QMO**	**25**	**100 mM $(NH_4)_2SO_4$**	**-**	**-**				
ATP	**3QXC**	20	100	A	+	10 mM 8-ac	10 mM ATP	10 mM $MgCl_2$	
GTP	**3QXJ**	20	150	A	-		10 mM GTP	10 mM $MgCl_2$	10 mM 8-ac
8-ac:ADP:PO_4^{3-}	**3QXH**	20	150	A	-		10 mM ADP	10 mM $MgCl_2$	10 mM 8-ac
ANP	**3QXS**	15	100	A	-		10 mM ANP	10 mM $MgCl_2$	10 mM 8-ac
8-ac:GDP:PO_4^{3-}	**3QXX**	20	100	C	+		10 mM GDP	10 mM $MgCl_2$	10 mM 8-ac
GDP: PO_4^{3-}	**3QY0**	20	150	A	-		10 mM GDP	10 mM $MgCl_2$	
8-ac:ADP:PO_4^{3-} (second crystal form)	**3MLE**	20	100	-	-	10 mM ATP, 10 mM $MgCl_2$, 10 mM 8-ac			

Table 2

Diffraction data collection and structural refinement parameters.

Complex	***apo***	**8-ac:ADP:PO_4^{3-} (second crystal form)**	**ATP**	**8-ac:ADP:PO_4^{3-}**	**GTP**	**ANP**	**8-ac:GDP:PO_4^{3-}**	**GDP: PO_4^{3-}**
PDB code	**2QMO**	**3MLE**	**3QXC**	**3QXH**	**3QXJ**	**3QXS**	**3QXX**	**3QY0**
Data collection								
Space group	*C*2	$P2_12_12_1$	*C*2	*C*2	*C*2	*C*2	C2	C2
a,b,c (Å)	82.1, 37.5, 69.6	79.77, 131.9, 133.1	81.9, 37.7, 69.2	81.5, 38.0, 68.8	82.2, 37.5, 69.1	82.1, 37.6, 69.2	81.9, 37.8, 68.8	81.7, 37.3, 69.1
β (°)α = γ = 90°	101.5	90	101.2	101.2	101.2	101.3	101.3	101.5,
Molecules per AU	1	6	1	1	1	1	1	1
Resolution (Å)	1.47 (1.47 - 1.52)	2.8 (2.8 - 2.85)	1.34 (1.34 - 1.36)	1.36 (1.36 - 1.38)	1.38 (1.38 - 1.40)	1.35 (1.35 - 1.37)	1.36 (1.36 - 1.38)	1.60 (1.60 - 1.63)
R_{merge}	0.069 (0.44)	0.099 (0.85)	0.04 (0.4)	0.026 (0.070)	0.050 (0.70)	0.035 (0.11)	0.061 (0.39)	0.062 (0.45)
I / σ(I)	48.8 (3.1)	21.6 (2.0)	35.1 (2.2)	47.3 (13.2)	35.8 (2.2)	46.8 (10.5)	29.5 (2.5)	19.2 (2.1)
Completeness (%)	99.0 (91.3)	99.9 (100)	98.1 (83.5)	97.7 (81.1)	98.6 (90.4)	97.7 (83.8)	98.1 (86.6)	99.7 (99.8)
Redundancy	7.7 (5.2)	7.7 (7.9)	3.6 (2.5)	4.0 (3.2)	3.9 (3.1)	3.8 (2.7)	3.8 (2.8)	3.8 (3.5)
Refinement								
Resolution (Å)	50.0 - 1.47	50.0 - 2.80	50.00 - 1.34	50.00 - 1.36	50.00 - 1.38	50.00 - 1.35	50.00 - 1.36	50.00 - 1.60
Number of reflections	35286	35281	45819	43544	42504	44773	43768	27374
R_{work} / R_{free}	14.8 / 17.9	20.1 / 24.6	13.8 / 17.3	11.7 / 14.2	15.9 / 17.9	14.3 / 16.5	13.0 / 16.2	13.9 / 17.1
Number of atoms								
Protein	1808	10345	1891	1863	1827	1879	1825	1802
Ligands/ions	2	289	97	65	63	80	76	88
Water	326	96	329	354	304	318	346	210
B factors								
Protein	18.6	60.0	16.3	10.4	16.5	12.8	13.8	15.1
Ligand/ion	28.3	55.4	30.1	16.6	28.1	25.7	26.8	31.8
Water	34.4	37.2	35.4	27.8	26	22.5	31.3	26
Structure quality								
R.m.s. Deviations								
Bond lengths (Å)	0.018	0.014	0.026	0.02	0.022	0.021	0.019	0.022
Bond angles (°)	1.7	1.4	2	1.7	1.9	1.8	1.7	1.8

FEBS J. Author manuscript; available in PMC 2013 March 01.

Complex	***apo***	**8-ac:ADP:PO_4^{3-} (second crystal form)**	**ATP**	**8-ac:ADP:PO_4^{3-}**	**GTP**	**ANP**	**8-ac:GDP:PO_4^{3-}**	**GDP: PO_4^{3-}**
PDB code	**2QMO**	**3MLE**	**3QXC**	**3QXH**	**3QXJ**	**3QXS**	**3QXX**	**3QY0**
Ramachandran Statistics								
Favored (%)	99.1	99.7	98.2	99.1	99.1	99.6	98.2	99.1
Additionally allowed (%)	0.9	0.3	1.8	0.9	0.9	0.4	1.8	0.9